

Optimized Bands: A New Design Concept for Concentrating Solar Parabolic Mirrors

Lifang Li¹

Ph.D. Candidate, ASME Student Member
School of Mechatronics Engineering
Harbin Institute of Technology
150001 Harbin, China.
lilifang2008@gmail.com

Andres Kecskemethy

Professor
Department of Mechanical Engineering
University of Duisburg-Essen
47057 Duisburg, Germany.
andres.kecskemethy@uni-due.de

A. F. M. Arif

Professor, Member of ASME
Department of Mechanical Engineering
King Fahd University of Petroleum & Minerals
31261 Dhahran, Saudi Arabia.
afmarif@kfupm.edu.sa

Steven Dubowsky

Professor, ASME Fellow
Department of Mechanical Engineering
Massachusetts Institute of Technology
Cambridge, 02139 MA.
dubowsky@mit.edu

Parabolic concentrator mirrors are an important component of many solar energy systems, particularly solar mirror collectors. Precision parabolic mirrors are expensive to fabricate and to transport. Here, a new concept for designing and fabricating precision parabolic mirrors is presented. The mirror is formed from a thin flat very flexible metal sheet with a highly reflective surface. Attached to the rear surface of the mirror sheet is a backbone band whose figure is optimized to form the reflective sheet into a precision parabola when its two ends are pulled toward each other. An analytical model to optimize the shape and thickness of the band is presented. The validity of the concept is demonstrated using Finite Element Analysis and laboratory experiments. The concept would permit flat mirror elements to be easily fabricated and efficiently packaged and shipped to field sites and assembled into the parabolic trough concentrators with potentially substantial costs reductions compared with conventional methods.

¹ Corresponding author, visiting Ph.D. student and research associate at Massachusetts Institute of Technology.

Keywords: Solar Collectors, Parabolic Mirrors, Low Cost Fabrication.

1. Introduction

1.1 Background

Solar mirror collectors are a major subsystem of many solar energy systems, particularly for solar thermal generators [1]. Large thermal systems may use many collectors covering large sites [2], see Fig. 1. Collectors generally consist of concentrating parabolic mirrors, an absorber tube and a supporting structure, which is often equipped with a solar tracking mechanism. They are called parabolic trough collectors (PTCs) [2], see Fig. 2.

The parabolic shaped mirror (reflector) focuses the sunlight onto a linear tube located at the mirror's focal line that contains a working fluid that absorbs the solar energy and carries it to some thermal plant, such as a Rankine or a Sterling heat engine [3]. The mirror is usually supported by a structure that often contains an active tracking mechanism that keeps the mirror pointed towards the sun, see Fig. 2.



Fig. 1: A Large Solar Mirror Collector Field Located at Kramer Junction, California, USA [2].

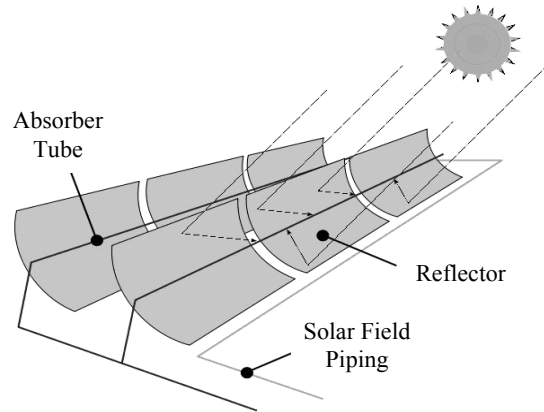
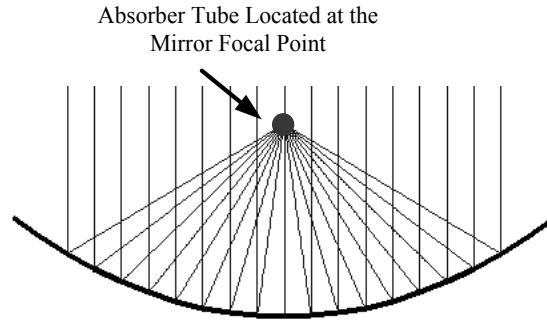


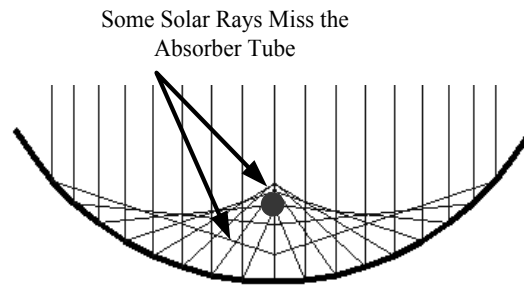
Fig. 2: Schematic of Solar Trough Collector [4].

The mirror shape must be precise enough to insure that the reflected sunlight is focused on the absorber tube. As shown in Fig. 3 and Fig. 4, it has been long known that if the shape of the mirror is not a parabola, the light will not precisely focus on a small tube [5]. There are important practical reasons to keep the absorber tube small, such as cost, thermal radiation and convection losses [6].

Mirror precision is important and conventional methods to fabricate precision parabolic mirrors are complex and costly. The reflectivity of the surface materials is an important factor in the optical efficiency. In solar energy applications, back silvered glass plates, anodized aluminum sheets and aluminized plastic films serve as reflectors. They are widely commercially available [7-9]. Films are usually adhered to a supporting material such as aluminum [10]. However the supporting material must be held with a precision parabolic shape by some supporting structures.



(a) Reflecting Mirror with Ideal Parabolic Cross Section



(b) Reflecting Mirror with Non-ideal Cross Section (Circular)

Fig. 3: Parabolic and Non-parabolic Mirror Cross Section.

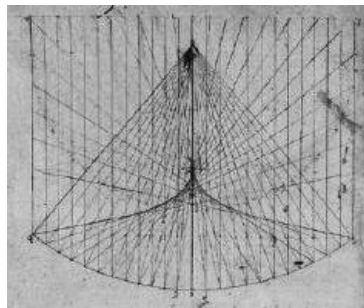
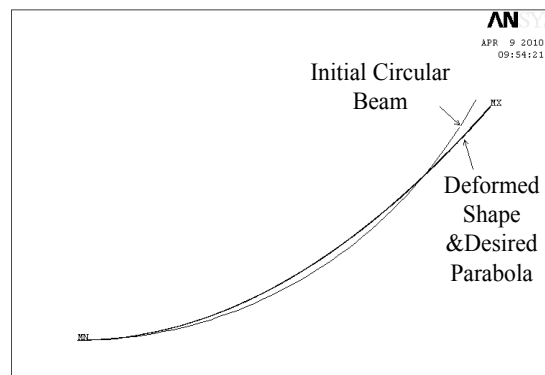


Fig. 4: Leonardo di Vinci Concave Mirror [5].

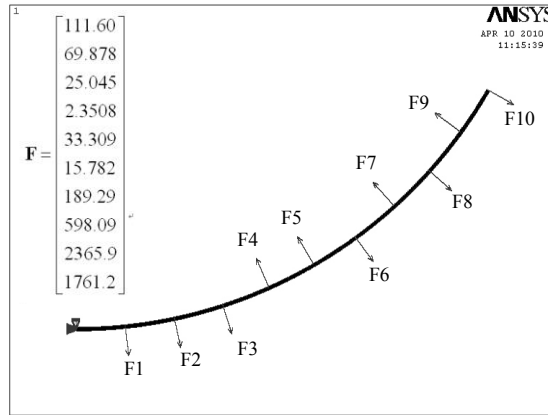
Parabolic dies or precision milled mirrors are usually required for these solar concentrators. However, they are often heavy and complex, which makes them unsuitable for rapidly deployable and portable systems. Moreover, their shape cannot be adjusted in real-time to compensate for thermal variations, etc. [11, 12].

Many future solar power plants will use very large numbers of parabolic mirror collectors, see Figure 1. Hence, methods to design precision parabolic mirrors at relative low cost, such as the one discussed in this paper, are potentially of great commercial importance [13-15].

In our past work, we have used distributed forces to form parabolas from simple circular shapes. Fig. 5 shows a set of distributed forces that will make an easily made a circular mirror into approximately parabolic shape. Fig. 5 (a) shows the shape adjustment required to forming a parabola from a rolled circular sheet material. Fig. 5 (b) shows an example of the required forces when 11 distributed forces are applied. While this approach can achieve the desired result, it requires far more forces than the 11 shown to achieve a smooth parabolic shape, and the implementation of the applied forces in the real system is very complex. A complete discussion of this work is beyond the scope of this paper, and the reader is referred to [16] for further details. Hence a new approach that is simpler to implement is presented in this paper.



(a) Finite Element Analysis

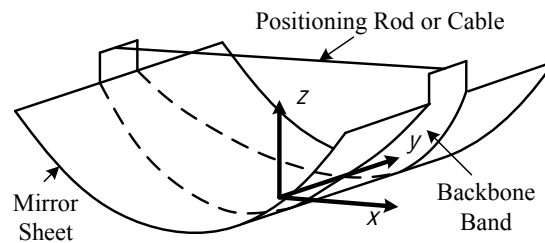


(b) Resulting Applied Forces (in N)

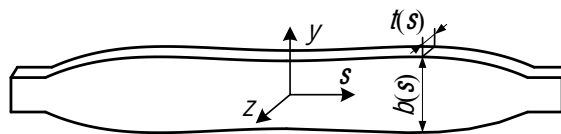
Fig. 5: Deforming a Circular Arc to a Parabola by Distributed Forces [16].

1.2 Approach and Summary

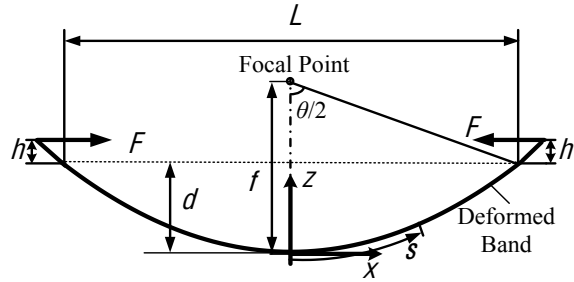
The new approach presented in this paper for designing and fabricating precision parabolic mirrors consists of a thin flat very flexible metal sheet with a highly reflective surface and a “backbone” band attached to its rear surface. The figure of the “backbone” band is optimized to form the sheet into a precision parabola when the two ends of the band are pulled toward each other by a predetermined amount. This can be achieved using a simple spacer rod or an active position control system when high precision requires real-time adjustment, see Fig. 6 (a).



(a) Band Mirror Concept



(b) Initial Flat Band with Varying Profile Cross Section



(c) Deformed Band Vertical Shape

Fig. 6: Band Mirror Concept.

Here, an analytical model is used to optimize the band's shape after it is deformed so that it is parabolic. The band is cut from a flat plate with a stiffness that is substantially higher than the mirror sheet. As discussed below, the elastic properties of the band can also be tuned to account for the mirror plate's stiffness.

It is also shown in this paper that the band profile can be determined numerically using Finite Element Analysis (FEA) combined with a numerical optimization method. These numerical results agree well with the analytical solutions.

Rather than optimizing the band stiffness by varying its width, its thickness, $t(s)$, can also be optimized to achieve the desired shape, see Fig. 6 (b). In some designs it may be desirable to vary both the band's thickness $t(s)$ and width $b(s)$ on the initial flat band. In general, varying the thickness, $t(s)$, would be a more costly manufacture than a uniform thickness band. However the thickness, as a function of length, $t(s)$, can be manufactured more simply by using a multi-layer band that approximates the variable thickness solution.

Moreover, the bands can also be optimized by punching holes on uniform width bands in approximately continuous patterns. However, this could create stress concentration problems in areas near the holes.

The backbone-band concept's validity is demonstrated in this paper by Finite Element Analysis and by laboratory experiments. In the experiments, mirror bands of various profiles are fabricated and tested in the laboratory using a collimated light source (that emulates direct sunlight) and outdoors in natural sunlight.

Our studies suggest that this concept would permit essentially flat mirror elements to be easily fabricated and efficiently packaged and shipped to field sites and then assembled into the parabolic mirrors for mirror solar collectors with potentially substantial cost reductions over current technologies.

2. Analytical Model Based on Euler-Bernoulli Beam Theory

Here a model of a flat band that will form a desired parabolic shape by moving its two ends toward each other to a given distance, L , is presented, see Fig. 6 (a). It is assumed that by proper selection of the bending stiffness $EI(s)$ of the band as a function of the distance, s , along its length a parabolic shape results when the band is deformed, where $I(s)$ is the second moment of area of the band and $E(s)$ is the modulus of elasticity of the band material.

For the analytical derivations, the following assumptions are made.

- The thickness $t(s)$ is much smaller than the length S of the band, so while the deflection is large (rotation and displacement), the shear stresses are small and hence Euler-Bernoulli beam equations can be used.

- The final distance L (parabolic chord length) between the two band ends is specified, and the rim angle of the desired parabola is given as θ , see Fig. 6 (c).
- The end deflection is achieved by the application of forces, F , during assembly and held in place by spacer rods, or an active control system.

2.1 Geometric Equations

If the focal length of the parabolic mirror is f , then the desired shape of the deformed band is given by the well-known relationship, see Fig. 6 (c):

$$z = \frac{x^2}{4f} \quad \left(-\frac{L}{2} \leq x \leq \frac{L}{2}\right) \quad (1)$$

The depth d of the parabola can be calculated as:

$$d = \frac{(L/2)^2}{4f} \quad (2)$$

Considering the energy efficiency of the mirror, a shallow parabola is selected, hence $d \leq f$. The rim angle θ of the parabola is given by:

$$\theta = 2 \arctan\left(\frac{L/2}{f-d}\right) \quad (3)$$

and the arc length s given by:

$$s(x) = \int_0^x \sqrt{1 + \left(\frac{u}{2f}\right)^2} du \quad (4)$$

where u is a dummy integration variable along the longitudinal direction of the beam.

Hence the initial flat band length S is given by:

$$S = 2 \int_0^{\frac{L}{2}} \sqrt{1 + \left(\frac{u}{2f}\right)^2} du \quad (5)$$

2.2 Band Bending Equations

Based on the above assumptions, Euler-Bernoulli beam theory applies, and the deflection of the beam are governed by [17]:

$$M(s) = EI(s) \frac{\partial \phi(s)}{\partial s} = EI(s) \kappa(s) \quad (6)$$

where $M(s)$ is the bending moment on the band, $\phi(s)$ is the rotation of band surface normal, and $\kappa(s)$ is the curvature of the final band shape, see Fig. 7.

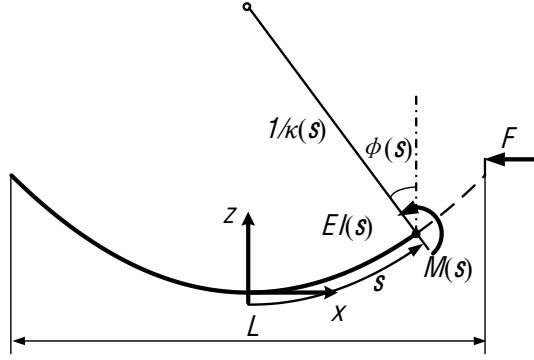


Fig. 7: Band Bending.

The curvature of the parabola $\kappa(s)$ is given by:

$$\kappa(s) = \frac{1}{2f} (1 + \ln^2(s/2f + \sqrt{s^2/4f^2 + 1}))^{-\frac{3}{2}} \quad (7)$$

From Equation (6), $I(s)$ is obtained as:

$$I(s) = \frac{M(s)}{E\kappa(s)} \quad (8)$$

With the thickness $t(s)$ and width $b(s)$ varying with length s , the second moment of area $I(s)$ for a rectangular cross section is given by:

$$I(s) = \frac{b(s)t^3(s)}{12} \quad (9)$$

As shown in Fig. 6 (c), the bending moment in the band can be calculated as a function of x

as:

$$M(x) = F \cdot \left(h + d - \frac{x^2}{4f} \right) \quad (10)$$

Thus, the bending moment along the band length s is governed by:

$$M(s) = F \cdot \left(h + d - f \cdot \ln^2 \left(\frac{s}{2f} + \sqrt{\frac{s^2}{4f^2} + 1} \right) \right) \quad (11)$$

2.3 Cross-Section Shaping for Achieving a Parabolic-Bended Band

It is well-known that loading a band with collinear external forces does not result in a parabolic shape. However, it is possible to shape the band's cross section to form a parabola shape when its ends are pulled together by horizontal forces.

In this process, it will be assumed that both the thickness and the bending stiffness of the thin mirror sheet are much smaller than the corresponding quantities of the band. In these cases, the shape can be tuned to a parabola by varying the band's thickness $t(s)$, its width $b(s)$ or both as a function of s , see Fig. 6 (b) (c). More general situations with non-negligible mirror sheet stiffness and/or bending stiffness can be considered by applying the Finite Element optimization method described in section 4.

a. Varying the Band Thickness

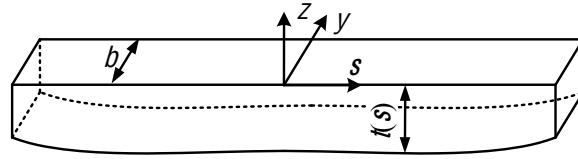
In this case, $t(s)$ changes and the width $b(s)$ is assumed to be a constant b , as shown in Fig. 8.

Thus, the thickness $t(s)$ as a function of the width b and the second moment of area the band is:

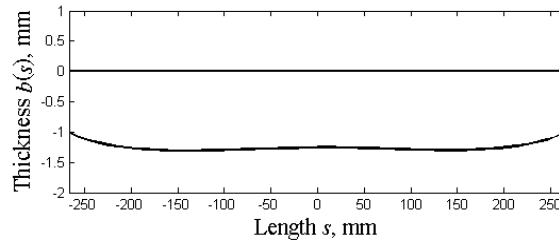
$$t(s) = \sqrt[3]{\frac{12 I(s)}{b}} \quad (12)$$

Substituting Equation (7), (8) and (11) into Equation (12) yields the thickness:

$$t(s) = \sqrt[3]{\frac{M(s)}{bE\kappa(s)}} = \sqrt[3]{\frac{12 F(h+d - f \ln^2(s/2f + \sqrt{s^2/4f^2 + 1}))}{bE\kappa(s)}} \quad (13)$$



(a) Varying Thickness



(b) Analytical Thickness

Fig. 8: Parabolic Band Obtained by Changing the Thickness

For a thick band, large shear stresses could result and produce non-negligible errors. Moreover, there might be an error induced by the difference of the curvature of the neutral line and the curvature of the upper surface. These errors are of second order and neglected in the present context. Also varying the thickness on the band is difficult and expensive to fabricate. A varying thickness can be approximated by constructing the band from layers, see Fig. 9. This laminating approach is probably not economically viable compared to the method discussed below.

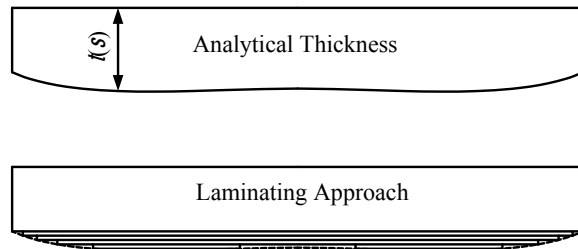


Fig. 9: Constructing the Variable Band Using Layers.

b. Varying the Band Width

A more cost-effective way to vary the area moment of inertia of the band is to vary its width as a function of s , $b(s)$, with the band's thickness, t , held constant, see Fig. 10. In this case, the band width is:

$$b(s) = \frac{12 I(s)}{t^3} \quad (14)$$

After substituting Equations (7), (8) and (11) into Equation (14), the ideal band width is obtained as the explicit solution:

$$b(s) = \frac{12 M(s)}{E t^3 \kappa(s)} = \frac{12 F(h+d - f \ln^2(s/2f + \sqrt{s^2/4f^2 + 1}))}{E t^3 \kappa(s)} \quad (15)$$

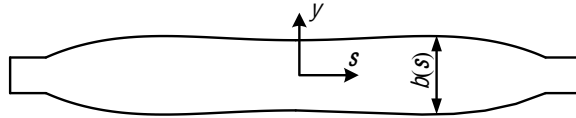


Fig. 10: Parabolic Band Obtained by Changing the Width

Such a design would be much easier to manufacture than a varying thickness design.

c. Combinations

Clearly it is possible to combine the above two approaches by varying both band thickness and width. This might be done when other design constraints need to be met.

The bands can also be optimized by punching holes on uniform width and thickness bands in approximately continuous patterns. However, the holes will produce a stress concentration problem.

In addition, it is clear that similar results can be achieved by varying the material properties

as a function of δ , though this does present some significant manufacturing challenges.

3. Mirror Performance Analysis

For this analysis, it is assumed that the mirrors are actively tracking the sun. In this case, the sunlight will be parallel to the axis of the parabola. The objective is to calculate the distance of the reflections of the rays from the focal point where the absorber tube will be mounted. The focal error, ϵ , is defined as the distance from the focal point to a reflection ray, see Fig. 11. This error determines the diameter of the absorber tube for the mirror to insure that all the solar energy intersects the absorber tube. Other metrics can be developed such as the percent of the energy that falls on a given absorber tube. The discussion of these metrics is beyond the scope of this paper.

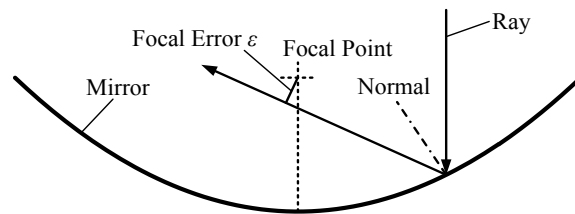


Fig. 11: Definition of Focal Error

Assuming small variations from the ideal parabolic profile, the focal error can be determined as follows (see Fig. 12).

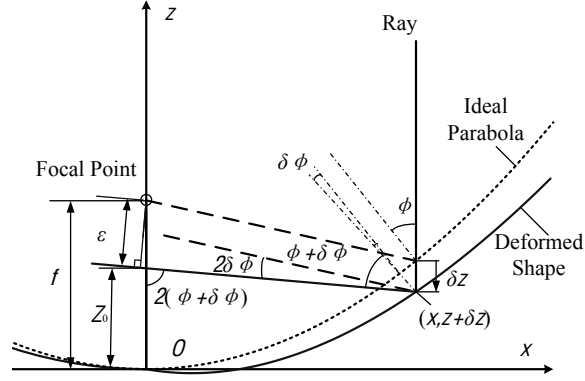


Fig. 12: Focal Error Analysis

For an arbitrary ray at horizontal position x , assume that the position error of the actual deformed shape is δZ , and that the angular error of the surface normal is $\delta\phi$. Taking Z as the vertical coordinate of the ideal parabola and X, Y as the running coordinates of the reflection ray, one obtains:

$$Z(X) = z + \delta Z - (X - x) \tan\left(\frac{\pi}{2} - 2\phi - 2\delta\phi\right) \quad (16)$$

When $X=0$, Z_0 is obtained as:

$$Z_0 = z + \delta Z - x \tan\left(\frac{\pi}{2} + 2\phi + 2\delta\phi\right) \quad (17)$$

The focal error is then obtained as:

$$\varepsilon(x, \delta Z, \delta\phi) = (f - Z_0) \sin(2(\phi + \delta\phi)) \quad (18)$$

As it can be seen, the focal error is positive when the reflected ray passes below the focal point and negative when it passes above the focal point.

The maximal focal error ε_{\max} is defined as the maximum of the absolute values of the focal errors for all rays entering the mirror's aperture.

The performance of solar concentrators is often expressed in terms of their ability to concentrate collimated light, called concentration ratio, \mathcal{C} , as a function of the chord length L and

the focal diameter d_F , 100% of light entering the mirror to reach the absorber tube. Here, for a given chord length, L , the maximum focal error, ε_{\max} , is chosen as a power precision performance metric.

4. FEA Shape Optimization

The analytical Euler-Bernoulli beam model shows the feasibility of the band-shaping approach for relative simple cases. A more general approach, suitable also for the treatment of more involved cases (e.g. non-negligible bending stiffness of mirror sheet), is to perform a numerical shape optimization procedure based on Finite Element Analysis (FEA), as discussed below.

The objective of the optimization is to minimize the maximum focal error by varying $l(\mathbf{s})$:

$$\min_{l(\mathbf{s})} \varepsilon_{\max} \quad (19)$$

In order to find the optimal profile $l(\mathbf{s})$, we describe it via a finite Fourier series expansion:

$$l(\mathbf{s}) = l_0 + \sum_{n=1}^N a_n \cos\left(\frac{n\pi \mathbf{s}}{L}\right) \quad (20)$$

where only even terms need to be regarded as the function $l(\mathbf{s})$ is symmetric with respect to \mathbf{s} .

The optimization task is to find the optimal coefficients

$$\mathbf{A} = [l_0 \quad a_1 \quad a_2 \quad \cdots \quad a_N] \quad (21)$$

such that when multiplied with the spatial shape vector:

$$\mathbf{B}(\mathbf{s}) = [1 \quad \cos(\pi \mathbf{s} / L) \quad \cos(2\pi \mathbf{s} / L) \quad \cdots \quad \cos(N\pi \mathbf{s} / L)]^T \quad (22)$$

the resulting area moment of inertia

$$l(\mathbf{s}) = \mathbf{A}\mathbf{B}(\mathbf{s}) \quad (23)$$

will minimize the maximal focal error ε_{\max} obtained after performing the corresponding FEA computation and evaluating the focal errors from the resulting bended band. This task corresponds to an unconstrained optimization problem with design variables A and cost function ε_{\max} , for which several well-known solution schemes exist. We chose here to apply an exact Newton search in which at each optimization step the Jacobian is computed by repeated evaluations of the FEA for small variations of each of the coefficients in A and the corresponding next estimate of $A^{(i)}$ is computed such that the linear approximation of the maximal focal error vanishes.

5. A Case Study

In this case study, a parabolic band based on varying width is presented. The optimization is obtained using both the analytical formulation in section 2 and the Finite Element based numerical optimization method in section 4. In this case, the rim angle θ is taken as 180° . Hence d is equal to f and L is equal to $4f$.

5.1 Analytical Band

Using the given parameters and Equation (15), the band width as a function of s is:

$$b(s) = \frac{12 F(h + f - f \ln^2(s/2f + \sqrt{s^2/4f^2 + 1}))}{E f^3 \kappa(s)} \quad (24)$$

With the parameters in Table 1, the ideal analytical shape shown in Fig. 13 is obtained.

Table 1: Band Parameters

Parameters	Value
Material	Spring steel
Focal length f (mm)	116.1
Rim angle θ (degree)	180

Chord length L	464.3 mm (18.3 inch)
Horizontal load F (N)	9.5
Load position h	25.4 mm (1 inch)
Young's modulus E (MPa)	210,000
Poisson's ratio	0.3
Thickness t	0.7937 mm (1/32 inch)

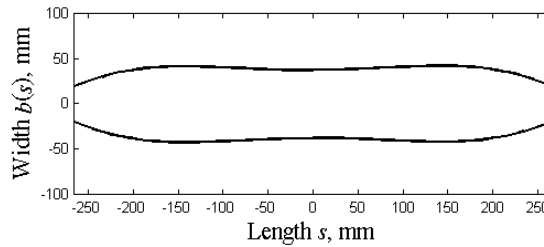


Fig. 13: Analytical Band Shape

A Finite Element model of the analytically shaped band was developed and implemented in ADINA [18-20]. Fig. 14 shows the boundary conditions and the force and moment loading of the FEA analysis.

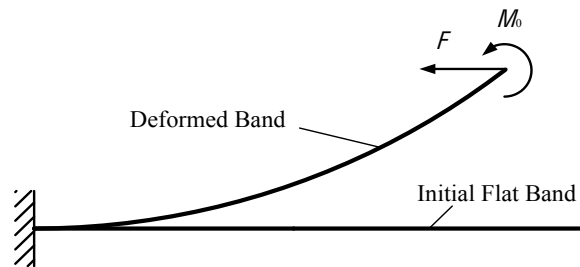


Fig. 14: Physical Model of FEA

The band is modeled as a shell bending problem. As shown in Fig. 15, U_1 , U_2 and U_3 are the translations about x , y and z axes, θ_1 and θ_2 are the rotations about x and y axes. The sign “ $\sqrt{}$ ” means the degree of freedom is active and “-” means it is fixed. Boundary conditions are shown at points B and C. The rotation about z axis is fixed for the whole model. In the model, it is assumed that the deformation is large and that strains are small, and that no plastic deformation occurs. The horizontal force, F , and the moment M_0 , which is equal to Fh , are divided into two

halves and applied as concentrated forces at the two end nodes. The loads were incrementally increased to the final value in 8 steps. The figure also shows the deflection and the stress distribution. The maximum equivalent Mises stress is 348.52 MPa (50536 psi shown in Fig. 15), which is below the yield stress of 1050 MPa for the chosen material (spring steel 38Si6).

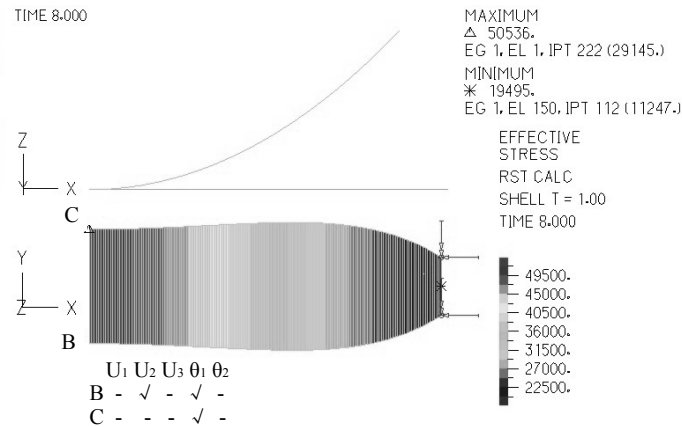


Fig. 15: Analytical Optimized Band FEA Results

To evaluate the precision of the result, ray tracing using the FEA deformed shape of the mirror was carried out, see Fig. 16. Assuming collimated rays entering the mirror along the axis of the parabola, the reflected rays are traced based on the normal rotations $\phi(\mathcal{S})$ and displacements $[\chi(\mathcal{S}) \mathcal{Z}(\mathcal{S})]$ from the FEA results.

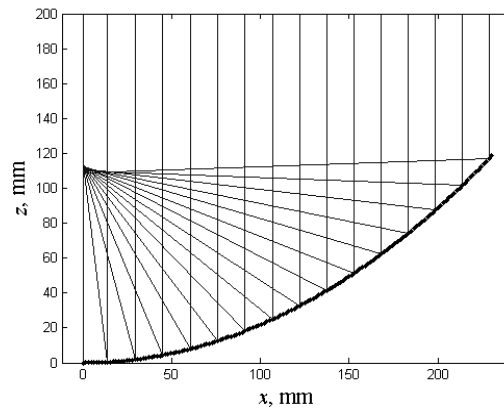


Fig. 16: Ray Tracing Using the FEA Results

The focal error is calculated using Equation (19). The resulting maximum error, ε_{\max} , for the analytically shaped band was 1.85 mm. This means the diameter of the absorber tube, d_F , should be at least 3.70 mm if 100% of the energy is to be absorbed.

5.2 FEA Optimized Band

The FEA results show that the band based on the analytical formulation is not a perfect parabola. A FEA optimized band was calculated using the shape optimization method from section 4. As initial guess, a rectangular band with width, b , 76.2 mm (3.0 inches) and thickness, t , 0.7937 mm (1/32 inch) was employed. The optimization procedure converged after 9 iterations with a termination condition of 10^{-4} for the magnitude of the increment ΔA of the design parameter vector.

Fig. 17 shows the band width $b(s)$ as a function of band length s for the optimized FEA and the analytical optimized results. It can be seen that the numerical FEA approach converges to a similar shape as the analytical approach.

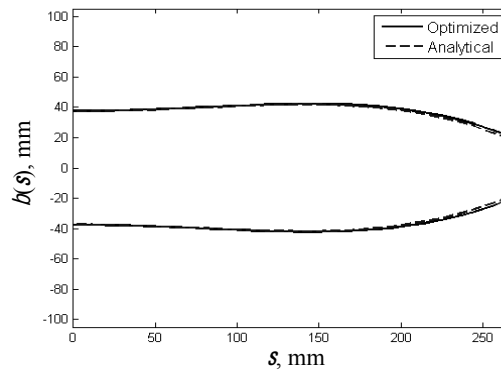


Fig. 17: FEA Optimized and Analytical Optimized Band

The ray tracing for the FEA optimized band is shown in Fig. 18. The maximum focal error is 0.38 mm, approximately a factor of five smaller than the idealized analytical result.

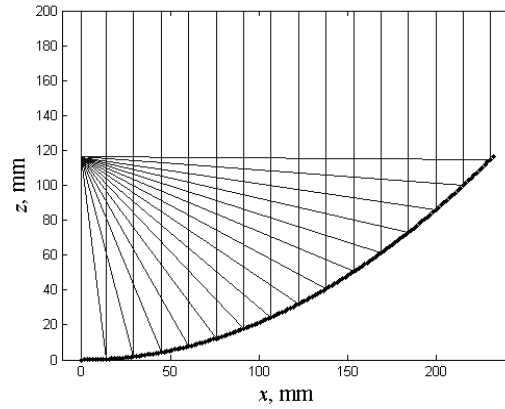


Fig. 18: Ray Tracing Using the FEA Optimized Band Results

5.3 Comparison with a Rectangular Band

In order to assess the improvement of solar energy collection properties of the shape-optimized band and a simple rectangular band, a FEA analysis of a rectangular band was carried out. The results shows that the maximal focal error of the optimized band is a factor of 10 smaller than that of the rectangular band, see Fig. 19.

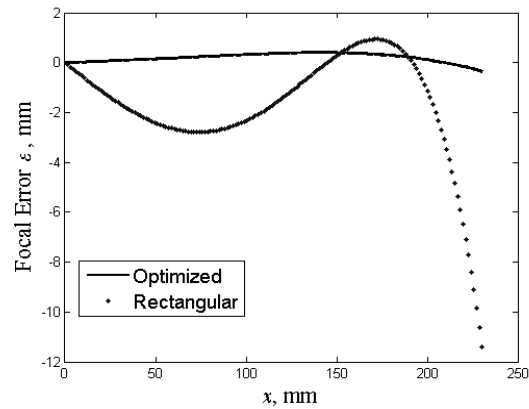


Fig. 19: Focal Error of Optimized and Rectangular Band

6. Experimental Validation

The results of the previous optimization were validated experimentally.

6.1 Experimental System

The experimental system consists of two main components: a flexible mirror with varying-width backbone band and a collimated light source consisting of a parabolic dish with an LED light source at its focal point and an absorber located on the mirror's focal line, see Fig. 20.

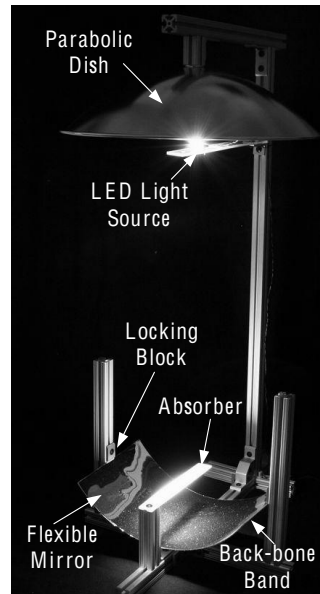


Fig. 20: Experimental System

Two locking blocks are used to construct the mirror's chord length, L , to its desired value. The concentration absorber was made from a semitransparent white plastic plate with the dimensions 1.5×26 inches.

The FEA optimized band was cut from a piece of 0.7937 mm (1/32 inch) spring steel sheet using a water jet cutter with tolerance ± 0.0254 mm ($\pm 1/1000$ inch). Fig. 21 shows the backbone band with optimized width and a simple rectangular band.

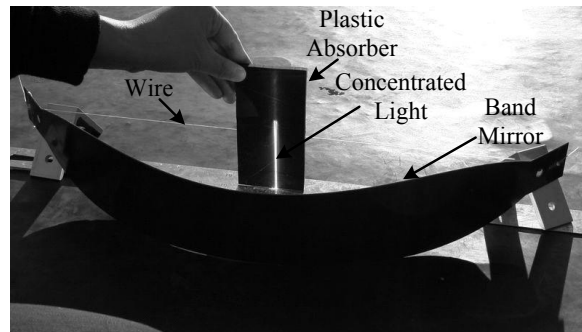


Fig. 21: Rectangular and Optimized Bands

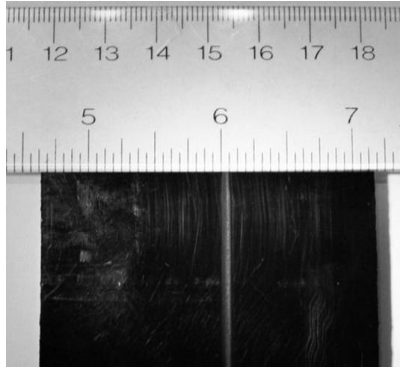
6.2 Experimental Results

Fig. 22 (a) shows the band mirror concentrating sunlight. A wire is used to fix the chord length, L , and a black plastic absorber was placed at the focal line of the band. The width of the focal area is less than 3 mm for 100% energy to be collected. The plastic absorber was quickly burnt by the concentrated light. The burn mark is shown in Fig. 22 (b). The width of burn is less than 2 mm. The concentration ratio of the optimized band, \mathcal{C} , is about 154.8 under sunlight. The result is much higher than those achieved by most current industrial parabolic mirror solar concentrators.

For comparison, the non-optimized rectangular band (see Fig. 21) had about 5 mm focal width with only about 90% energy collected. It was not possible to measure the focal width of 100% collection as the image was outside of the measurement limits.



(a) Band Mirror Concentrated Sunlight



(b) Burn Mark by Focal Line on Plastic Absorber

Fig. 22: Sun Light Concentrated by the Band Mirror

The focal width of the optimized band is 4.6 mm measured in the laboratory for 100% of the rays collected. And the rectangular band focal width is 10.3 mm with about 90% rays collected.

6.3 Parabolic Shape Measurement

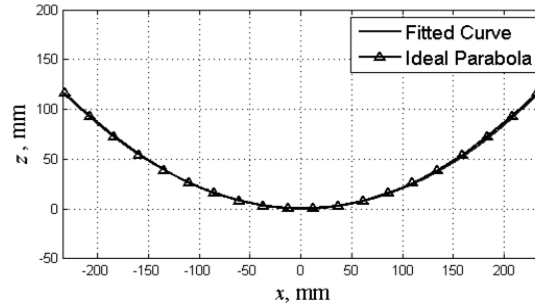
The parabolic shape of the deformed band was measured in two ways, an edge finder on a CNC milling machine and an optical method.

However, since the band was thin and thus highly compliant, the edge finder induced deformation errors that made the measurements unfit for focal error determination.

Thus, the optical method, in which no physical contact is made with the band, was further pursued. In this method, a photograph of the band on the vertical direction was taken and converted into a monochrome image (black and white). The threshold figure yields a high contrast black and white digital image, see Fig. 23 (a). This image was then fitted with a high degree polynomial function and thus yielded a shape that closely matched the predicted contour, see Fig. 23 (b).



(a) Threshold Image



(b) Comparison of Fitting Curve and Predicted Contour

Fig. 23: Optical Method of Measurement

As before, the shape was used as the ray tracing algorithm, see Fig. 24. The focal error was obtained, see Fig. 25. Note that any measured rigid body rotations and translations of the mirror shape in Fig. 25 due to calibration issues have been eliminated from the results shown. The maximum focal error is small, 0.72 mm, compared with 6.41 mm of the rectangular band.

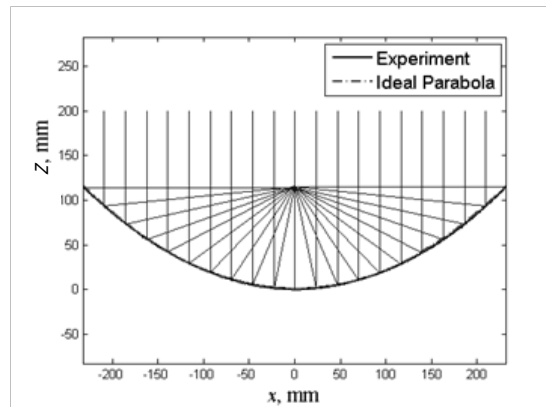


Fig. 24: Ray Tracing Using Optical Method

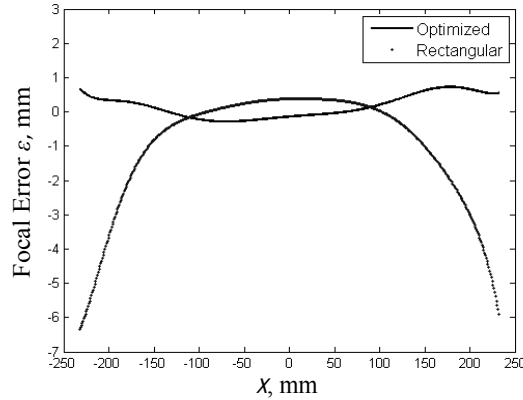


Fig. 25: Focal Error Using Optical Method

7. Results and Conclusions

In this paper, the design and manufacture of a simple and low cost precision parabolic mirror solar concentrator with an optimized profile backbone band is presented. The band is optimally shaped so that it forms a parabola when its ends are pulled together to a known distance. It could be fabricated and shipped flat, and onsite its ends would be pulled together to distance by a wire, or rod, or actively controlled with a simple control system. Varying width of the band as a function of its length appears to be the most cost-effective way to fabricate the band. A method for calculating the optimized profile band is presented using an analytical model and Finite Element Analysis. The backbone band was experimentally evaluated using the metric of the maximum focal error and focal width. The experimental results showed a factor of 10 improvement in the performance of optimized band compared to a simple rectangular band.

We expect that this approach would be a cost-effective and simple technology for the design and fabrication of high precision parabolic mirror solar concentrators for solar energy applications.

Acknowledgments

The assistance in this study of Prof. Klaus-Jurgen Bathe, Mr. Roman Geykhman, Dr. Jekanthan Thangavelautham, Ms. Amy Bilton, Ms. Leah Kelley and Dr. Francesco Mazzini, all of MIT is gratefully acknowledged. The authors thank the King Fahd University of Petroleum and Minerals in Dhahran, Saudi Arabia, for funding the research reported in this paper through the Center for Clean Water and Clean Energy at MIT and KFUPM.

Nomenclature

- a_n = shape coefficients
- A = shape coefficients vector
- $A^{(i)}$ = the i^{th} step of shape coefficients vectors of optimization
- $B(s)$ = shape vector respect to s axis (mm)
- $b(s)$ = band width with respect to s axis (mm)
- $b(x)$ = band width with respect to x axis (mm)
- C = solar concentration ratio (dimensionless)
- d = depth of PTC (mm)
- d_F = diameter of focal area (mm)
- E = Young's modulus (MPa)
- f = focal length (mm)
- F = horizontal force (N)
- h = force position (mm)
- I_0 = initial second moment of area of rectangular band (m^4)
- $I(x)$ = second moment of area respect to x axis (m^4)
- $I(s)$ = second moment of area respect to s axis (m^4)
- L = parabolic chord length (mm)
- $M(x)$ = bending moment respect to x axis (MPa)
- $M(s)$ = bending moment respect to s axis (MPa)
- s = band arc length (mm)
- S = initial flat band length (mm)
- x, y, z = Cartesian coordinates
- X, Y, Z = Cartesian coordinates

Greek symbols

- δz = band shape error on z direction (mm)
- $\delta \phi$ = normal angle error (rad)

- ε = focal error (mm)
- ε_{\max} = maximum focal error (mm)
- θ = rim angle (deg)
- $\phi(s)$ = rotation of band normals from flat (rad)

References

- [1] Romero M., Martínez D. and Zarza E., 2004, “Terrestrial Solar Thermal Power Plants: On the Verge of Commercialization”, 4th Int. Conf. on Sol. Power from Space, Granada, pp.81-89.
- [2] “Solar Energy System Design”, <http://www.powerfromthesun.net/chapter1/Chapter1.htm>.
- [3] Quaschnig V., Muriel M. B., 2001, “Solar Power - Photovoltaics or Solar Thermal Power Plants?”, VGB Congress Power Plants, Brussels.
- [4] http://commons.wikimedia.org/wiki/File:Parabolic_trough.svg.
- [5] Leonardo da Vinci, 1474-1518, “The Codex Arundel”, The British Library, London.
- [6] Hatwaambo S., Hakansson, H. J. Nilsson and Karlsson B., 2008, “Angular Characterization of Low Concentrating PV–CPC Using Low-cost Reflectors”, Solar Energy Materials and Solar Cells, Volume 92, Issue 11, pp. 1347-1351.
- [7] Thomas A. and Guven H. M., 1993, “Parabolic Trough Concentrators design, Construction and Evaluation”, Energy Convers. Mgmt, Vol. 34, No. 5, pp. 401-416.
- [8] Kennedy C., Terwilliger K., Milbourne M., 2005, “Development and testing of solar reflectors”, Conference Paper NREL Report CP-520-36582, Golden CO.
- [9] Kennedy C., Terwilliger K., 2005, “Optical Durability of Candidate Solar Reflectors”, Journal of Solar Energy Engineering, Vol. 127, No. 2, pp. 262-269.
- [10] <http://www.reflectechsolar.com/home.html>.

- [11]A. Fernández-García, Zarza E., Valenzuela L. and Pérez M., 2010, “Parabolic-mirror Solar Concentrators and Their Applications”, *Renewable and Sustainable Energy Reviews*, Volume 14, Issue 7, 2010, pp. 1695–1721.
- [12]Winter C.J., Sizman R. and Vant-Hull, L. 1991, “Solar Power Plants—Fundamentals, Technology Systems and Economics”, Springer-Verlag, Berlin.
- [13]Price H., Lüpfert E., Kearney D., Zarza E., Cohen G. and Gee R. et al.,2002, “Advances in Parabolic Mirror Solar Power Technology”, *J Sol Energy Eng* 124, pp. 109–117.
- [14]Geyer M., Lüpfert E., Osuna R., Esteban A., Schiel W. and Schweitzer A. et al., 2002, “EUROMIRROR—Parabolic Mirror Concentrator Developed for Cost Efficient Solar Power Generation”, *Solar PACES*, 11th Int. Symp. On Conc. Sol. Power and Chem. Energy Technol., Zurich.
- [15]Kearney D.W., 2007, “Parabolic Mirror Collector Overview”, In: *Parabolic Mirror Workshop at the NREL*.
- [16]Pashah S., Arif A. F. M., 2010, “FE Simulation of a Parabolic Collector”, *Stress Analysis Laboratory Report*, King Fahd University of Petroleum & Minerals, Dhahran, Saudi Arabia.
- [17]Mutyalarao M., Bharathi D., Nageswara Rao B., 2010, “Large deflections of a cantilever beam under an inclined end load”, *Appl. Math. Comput.*, doi:10.1016/j.amc.
- [18]K. J. Bathe, 1996, *Finite Element Procedures*, Prentice Hall.
- [19]D. Chapelle, K. J. Bathe, 2003, *The Finite Element Analysis of Shells – Fundamentals*, Springer.
- [20]ADINA R&D, Inc, 2000, *ADINA User Interface Primer*. ADINA R&D, Inc.